3 Carbon Nanotubes and Nanotube-Based Composites: Deformation Micromechanics

Robert J Young and Libo Deng

School of Materials, University of Manchester, Manchester, M13 9PL, UK

3.1. Introduction

The pioneering work upon the two-dimensional graphene, a one-atom thick planar sheet of sp^2-bonded carbon atoms, was awarded the Nobel Prize in Physics in 2010. Carbon nanotubes (CNTs) are related nanostructures that can be envisaged as being made by rolling the two-dimensional graphene sheets into cylinders. This gives rise to fascinating materials, which have been attracting great deal of research interest in the last two decades, due to their impressive properties and wide range of potential applications. Their applications in mechanical reinforcement and electronic device are particularly promising. The excellent mechanical properties of nanotubes are related to the strong sp^2 hybridized carbon-carbon bonds and the perfect hexagonal structure in the graphene sheet from which they are built up, while the unique electronic properties are due largely to the one-dimensional confinement of electronic and phonon states which results in van Hove singularities in the density of states (DOS) of nanotubes (Dresselhaus et al., 2005).

Raman spectroscopy has become an important technique to both characterise the electronic structure and follow the deformation behaviour of CNTs. This technique provides insight into their intrinsic properties and the interaction of nanotubes with the surrounding environment, as well as the mechanical reinforcing efficiency of nanotubes in composites.

This chapter aims to give a brief introduction to the structure, preparation and properties of carbon nanotubes, and to review the background and main properties of nanotube Raman bands, with an emphasis on the effect of deformation upon the Raman bands. More comprehensive reviews on the physical properties and Raman spectroscopy of CNTs can be found elsewhere (Dresselhaus et al., 2002 and Dresselhaus et al., 2005).

3.2. The Preparation, Structure and Properties of CNTs

3.2.1. Preparation

Three methods are employed widely to prepare nanotubes: arc-discharge, laser ablation, and chemical vapour deposition (CVD) (Moniruzzaman and Winey, 2006).

O. Paris (Ed.), *Structure and Multiscale Mechanics of Carbon Nanomaterials*,
CISM International Centre for Mechanical Sciences
DOI 10.1007/ 978-3-7091-1887-0_3

The first two methods involve the condensation of hot gaseous carbon atoms generated from the evaporation of solid carbon, while in the CVD process, a gaseous carbon source is decomposed catalytically and the nanotubes are deposited on a substrate or grown from a substrate. Catalytic-grown nanotubes have fewer impurities but have more defects than the arc-grown nanotubes. The arc-grown CNTs are therefore mechanically stronger than the CVD-CNTs, but the latter will almost certainly find more applications. This is because the length and structure are more controllable in a CVD process, and this process is also more amenable to being scaled-up for industrial production (Moniruzzaman and Winey, 2006).

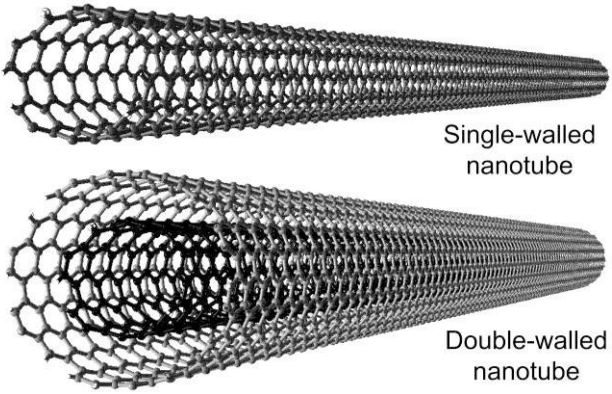

Figure 3.1. Schematic representations of single- and double-walled carbon nanotubes. Multi-walled nanotubes can have up to 20 layers of nested tubes. (Courtesy of Dr F. Ding, Hong Kong Polytechnic University). (Adapted from Young and Lovell, 2011 with permission from CRC Press).

3.2.2. Structure

CNTs are long cylinders of covalently bonded carbon atoms. The carbon atoms are arranged on a hexagonal network and each of them has three neighbours with which they form strong sp^2 hybridized carbon-carbon bonds. There are basically two main types of carbon nanotubes according to the numbers of graphene cylinder in their structure as shown in Figure 3.1: single-wall nanotubes (SWNTs) and multi-wall nanotubes (MWNTs); double-wall nanotubes (DWNTs) are a special case of MWNTs (Saito et al., 1998).

An SWNT can be considered as a seamless roll of a single graphene sheet. The nanotube is one atom in thickness (which is 0.34 nm), tens of atoms in circumference, and up to a few millimetres in length. The different ways of rolling graphene into

tubes are described by the chirality as defined by the circumferential vector (Saito et al., 1998; Moniruzzaman and Winey, 2006)

$$\vec{C}_h = n\vec{a}_1 + m\vec{a}_2 \tag{3.1}$$

where n and m is the length along the unit vectors of the two lattice vectors, respectively, as shown in Figure 3.2. MWNTs are made of many coaxial single-wall nanotubes with an interlayer separation of 0.34 nm, and each of the walls may possess different chiralities.

The diameter and chiral angle are two important parameters that define the nanotube structure, which can be derived from the chirality indices (n, m). The diameter d_t is given by:

$$d_t = a_0\sqrt{(n^2 + nm + m^2)}/\pi \tag{3.2}$$

where a_0 is the length of lattice vector and has a value of 0.249 nm. The chiral angle Φ is defined as the angle between the chiral vector and the zigzag direction x (Figure 3.2). It varies in the range of 0 - 30º and is given by:

$$\Phi = \tan^{-1}\frac{\sqrt{3}n}{2m+n} \tag{3.3}$$

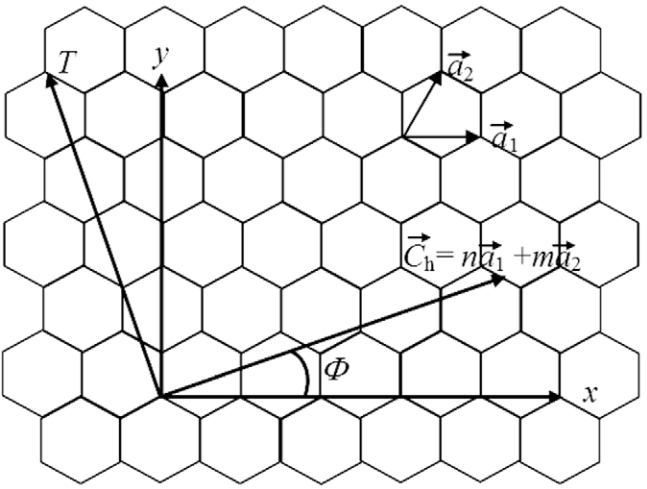

Figure 3.2. Schematic diagram of a graphene sheet showing the chiral vectors.

3.2.3. Properties

The high aspect ratio, the strong sp^2 carbon-carbon bonds, and the one-dimensional confinement of electronic states, confer CNTs with a range of interesting physical properties such as unique electronic properties, excellent mechanical properties, and good thermal conductivity and electrical conductivity.

SWNTs behave as either semiconductors or metals, depending on the remainder of (n-m) divided by 3: those with n-m = 3k are metallic nanotubes while those with n-m = 3k±1 are semiconducting nanotubes (where k is integer) (Moniruzzaman and Winey, 2006). Therefore, approximately one third of SWNTs are metallic and the rest are semiconducting. For semiconducting nanotubes, the band gap decreases as the diameter increases.

Deformation has a significant effect on electronic structure of nanotubes. The effect of strain on the electronic structure depends on the deformation mode (i.e. uniaxial strain, torsional strain or radial deformation) and nanotube chirality. For example, uniaxial strain opens the band gap of non-armchair metallic nanotubes but has no effect on armchair nanotubes. Torsional strain can change the electronic structure of armchair nanotubes but does not affect zigzag nanotubes.

Nanotubes and graphite share the same hexagonal network of sp^2 carbons in their structure. Mechanical properties of nanotubes are therefore expected to be comparable with graphene which has in-plane Young's modulus of 1.06 TPa and strength of 130 GPa (Coleman et al., 2006a, 2006b). In fact, some computer simulation work soon after the discovery of nanotubes did predict similar mechanical properties to those of graphene (Lu, 1997). The first actual mechanical measurement on nanotubes was performed using transmission electron microscopy (TEM) (Treacy et al, 1996). Since then, bending tests using an atomic force microscopy (AFM) tip have been developed and used widely (Wong et al., 1997). A Young's modulus for SWNTs of 1.0 TPa and 0.3 - 0.9 TPa for MWNTs, and tensile strength of 50 - 150 GPa for SWNTs and 10 - 50 GPa for MWNTs are generally quoted by the scientific community. The actual values vary from nanotube to nanotube, cover a wide range, and depend on many factors such as the nanotube type, preparation method, purity and diameter.

Theoretical work has predicted a very high thermal conductivity for CNTs, of approximately 6000 W m^{-1} K^{-1}, while experimental work has recorded a value of 3000 W m^{-1} K^{-1}. MWNTs have been found to also exhibit good electrical conductivity, which is in the range of 10^6 - 10^7 S/m (As a comparison, the copper has a thermal conductivity of 400 W m^{-1} K^{-1} and electrical conductivity of 6×10^7 S/m). The physical properties of CNTs and a comparison with typical engineering materials are summarized in Table 3.1.

Table 3.1. Physical properties of CNTs compared with other engineering materials

Material	Mechanical properties		Thermal conductivity ($W\ m^{-1}\ K^{-1}$)	Electrical conductivity (S/m)
	Modulus (GPa)	Strength (GPa)		
Carbon nanotubes	1000	30 - 100	>3000	10^6 - 10^7
Carbon fibre (Pitch)	300 - 700	5 - 7	1000	2 - 8.5×10^6
Copper	110 - 128		400	6×10^7

3.3. Raman spectroscopy of SWNTs

The Raman spectroscopy of CNTs has becoming an important research topic since the first work was published in 1997. This technique is particularly useful for investigation of the properties of SWNTs due to the resonance effects and the discussion in the following section is confined to SWNTs only.

Four characteristic Raman bands, namely the radial breathing modes (RBMs), G-band, D-band and 2D -band (also called the G'-band) carry a large amount of structural information and have been studied in most detail, although several other weaker and broader features have also been observed in the nanotube spectra. A typical Raman spectrum of SWNTs is shown in Figure 3.3.

3.3.1. Radial Breathing Modes

The RBM features appear between 100 and 500 cm^{-1}, and are vibrational modes in which all the carbon atoms move radially, perpendicular to the nanotube axis, as if the nanotube was breathing. The lineshape of the RBM peak for a single nanotube is a simple Lorentzian line and the natural linewidth is 3 cm^{-1}. The RBM peak is quite often broadened to exhibit a linewidth of 4 - 10 cm^{-1} due to the interaction of nanotubes with the environment (Dresselhaus et al., 2005).

The RBM frequency ω_{RBM} is independent of the chiral angle Φ but depends linearly on the reciprocal nanotube diameter d_t through the relation (Dresselhaus et al., 2002 and Dresselhaus et al., 2005):

$$\omega_{\mathrm{RBM}} = \frac{A}{d_t} + B \tag{3.4}$$

where the parameters A and B (B is associated with the effect of environment on the ω_{RBM}) are determined experimentally. Although the form of the relation is well established, a variety of values for the parameters A and B have been found by different groups with different samples. The interaction with the different environments leads to each sample having its own set of parameters to determine d_t from ω_{RBM}. Table 3.2 summarizes the values for the ω_{RBM}/d_t relation reported in the literature.

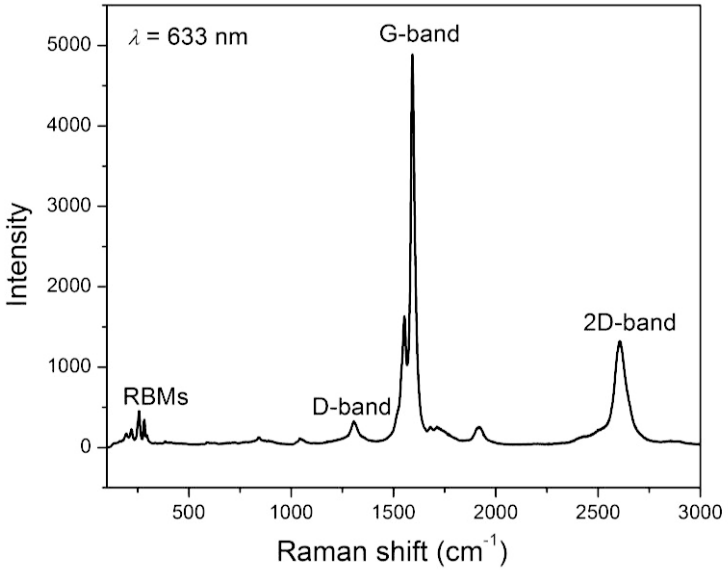

Figure 3.3. A typical Raman spectrum of SWNTs showing the four characteristic bands.

Table 3.2. A and B values for Equation (3.4) reported in the literature.

Sample	A	B	Reference
SWNTs on a silicon substrate	248	0	Jorio et al., 2001
SDS-dispersed HiPco SWNTs	223.5	12.5	Bachilo et al., 2002
SDS-dispersed HiPco SWNTs	218	17	Fantini et al., 2004
Alcohol-assisted CVD-SWNTs	217	15	Araujo et al., 2007
Laser ablation bundled SWNTs	232	0	Milnera et al., 2000

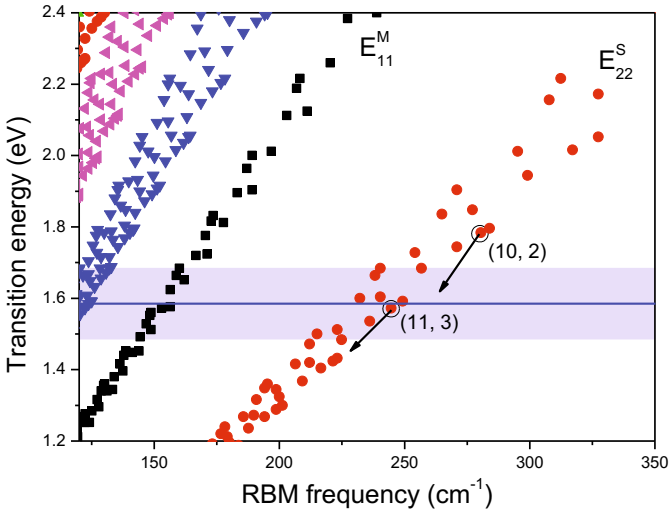

Figure 3.4. A theoretical Kataura plot for individual SWNTs. The blue box indicates a resonance window for an excitation laser with energy of 1.58 eV. The arrows indicate the down-shift of E_{22}^{S} for two individual nanotubes when they aggregate into bundles, showing the roping effect on RBMs. All E_{ii} values were calculated using a nearest-tight binding model.

The most important information one can determine from the RBMs is the nanotube chirality, which is given by the (n, m) indices. The identification of the (n, m) indices is based on resonance theory which gives rise to the so-called Kataura plot which is a plot of interband transition energy E_{ii} versus nanotube diameter (or ω_{RBM}) (Kataura et al., 1999). The diameter can be determined from ω_{RBM} using Equation (3.4). The interband transition energy E_{ii} for the Kataura plot can be determined using resonance Raman spectroscopy equipped with a tunable laser (this method gives a precision of 3 meV for each E_{ii}), photoluminescence spectroscopy (with the precision of 20 - 30 meV) and theoretical approaches (Bachilo et al., 2002 and Fantini et al., 2004).

The value of E_{ii} is influenced by many factors such as whether the nanotubes are in bundles or isolated, whether they are wrapped by surfactants, the type of solvent in which nanotubes are dispersed, the type of substrate and the temperature. As for the influence of intertube interaction, the E_{ii} value shifts to lower energies and RBM peaks shift to lower frequencies by 1 - 10 cm^{-1} when isolated individual nanotubes aggregate into bundles. Theoretical studies predicted that the value of E_{ii} can shift as much as 0.25 eV upon bundling (O'Connell et al., 2004), and they determined ex-

experimentally an average value of 86 meV for the down-shift. The down-shift of the E_{ii} may lead to the so-called "roping effect" on RBM peaks, that is, some RBMs that are seen in the isolated state disappear when in bundles (there is an opposite case: some RBMs that are absent for isolated nanotubes appear when they are in bundles) (Doorn et al., 2003 and Heller et al., 2005). Figure 3.4 illustrates the roping effect upon two nanotubes: the (10, 2) and (11, 3) nanotubes that are off resonance and in resonance with a 785 nm laser, respectively, when isolated, are brought into and outside the resonance window when in bundles due to the changes of E_{ii}.

The uncertainties in E_{ii} values and $\omega_{\mathrm{RBM}}/d_{\mathrm{t}}$ relation bring difficulty in identifying nanotube chirality. Additional information for identification of nanotube chirality can be provided by deforming nanotubes which affects the electronic structure and consequently the Raman bands. Lucas and Young (2007) managed to assign a unique nanotube structure to each RBM separated by just 1 - 2 cm^{-1} by studying the effect of deformation upon the RBM intensity.

3.3.2. G-band

The G-band originates from the vibrations of neighbouring carbon atoms in opposite direction along the nanotube axis and its circumference and is observed in the 1500 - 1605 cm^{-1} region for SWNTs. In most cases, the G-band can be fitted with two most intense peaks labeled by G^+, for atomic vibration along the tube axis; and G^-, for modes with atomic vibration along the circumferential direction (Dresselhaus et al., 2002). ω_{G^+} is independent of the diameter while ω_{G^-} decreases with the decreasing diameter. The dependence of ω_{G} on nanotube diameter is given by:

$$\omega_{\mathrm{G}^-} = \omega_{\mathrm{G}^+} - \xi / d_{\mathrm{t}}^2 \tag{3.5}$$

where ξ has a value of 47.7 nm^2 cm^{-1} and 79.5 nm^2 cm^{-1} for semiconducting and metallic nanotubes, respectively (Dresselhaus et al., 2005). This equation allows the determination of nanotube diameter when the RBM is absent, although the information is less accurate than direct RBM measurement.

The lineshape of the G-band of semiconducting SWNTs is quite different from that of metallic nanotubes. Specifically, the difference in G^- lineshape allows one to readily distinguish between semiconducting and metallic nanotubes (Dresselhaus et al., 2002). For semiconducting nanotubes both the G^+ and G^- peaks are of a Lorentzian profile with linewidths of 6 - 15 cm^{-1}, whereas for metallic nanotubes, the G^+ peak has a Lorentzian lineshape similar to the semiconducting tubes, but the G^- peak is a broad and asymmetry peak and is usually fitted using a Breit-Wigner-Fano (BWF) function (Dresselhaus et al., 2002). The BWF broadening is related to free electrons in nanotubes with metallic character. There are however conflicting reports in the G^- lineshape of metallic nanotubes. Paillet et al. (2005) demonstrated

BWF line is an intrinsic feature of metallic nanotube bundles but the BWF component vanishes in isolated metallic nanotubes. In contrast, Bose et al. (2005) predicted the BWF lineshape to be intrinsic in single metallic nanotubes.

Interacting with the environment can also influence the G-band of nanotubes significantly. Important environmental factors include the aggregation state (i.e. isolated nanotube or bundles), the charge transfer arising from doping a SWNT and the substrate. For SWNTs debundled with the assistance of dispersant, the dispersant molecules wrapping the nanotube can suppress the vibration in the circumferential direction, giving rise to a weak G^- peak (Kawamoto et al., 2006). In addition, the G^+ linewidth is lower for individual nanotube than for nanotube bundles. As for the influence of charge transfer, removing charge from a SWNT (i.e. p-doping or oxidizing) leads to an up-shift of the G^+ peak around 1592 cm^{-1}, while adding charge (i.e. n-doping or reducing) to a SWNT results in a down-shift (Wise et al., 2004).

3.3.3. D-band and 2D-band

The D-band and its second order overtone 2D-band (also called 2D band) are observed in the 1250 - 1450 cm^{-1} and 2500 - 2900 cm^{-1} regions, respectively. The D-band scattering involves one-phonon emission while the 2D-band scattering involves emission of two phonons. The causes of these two bands both involve a double resonance Raman process as shown in Figure 3.5. The D-band scattering consists of one-elastic and one-inelastic scattering process, in which the elastic scattering arises from defects (such as vacancies, impurities and hetero-atoms) in the crystal. On the other hand, the 2D-band is due to two-inelastic scattering process, in which the two emitted phonons possess vectors of $+\boldsymbol{q}$ and $-\boldsymbol{q}$, respectively. The momentum constant is therefore automatically preserved and no defect is required to observe the 2D-band.

The D- and 2D- bands are known as dispersive bands because they change their frequencies when the laser excitation energy changes. For example, a function $\omega_{2D}=2420+106E_{laser}$ has been found for the dependence of 2D-band position upon E_{laser} (Dresselhaus et al., 2002). The dependence of ω_D and ω_{2D} on E_{laser} is due to the dependence of phonon energy on E_{laser}.

Both the ω_D and ω_{2D} are found to be dependent also on both the nanotube diameter d_t and the chiral angle Φ, a property unique to nanotubes. The diameter dependence is a more complex issue. When considering the ω_{2D}/d_t dependence in a broad range of d_t where different E_{ii} interband transitions are involved in resonance, the value of the ω_{2D} decreases as the d_t decreases and follows the relation: $\omega_{2D}= 2708.1-35.4/d_t$. On the other hand, when analysing the data within the same interband transition where the d_t varies over a small range, ω_{2D} decreases with increasing d_t through the dependence: $\omega_{2D}= \omega_0+C_i/d_t$, where the parameter C_i has a value of 34 nm cm^{-1} for E_{33}^S and 182 nm cm^{-1} for E_{44}^S (Filho et al., 2003).

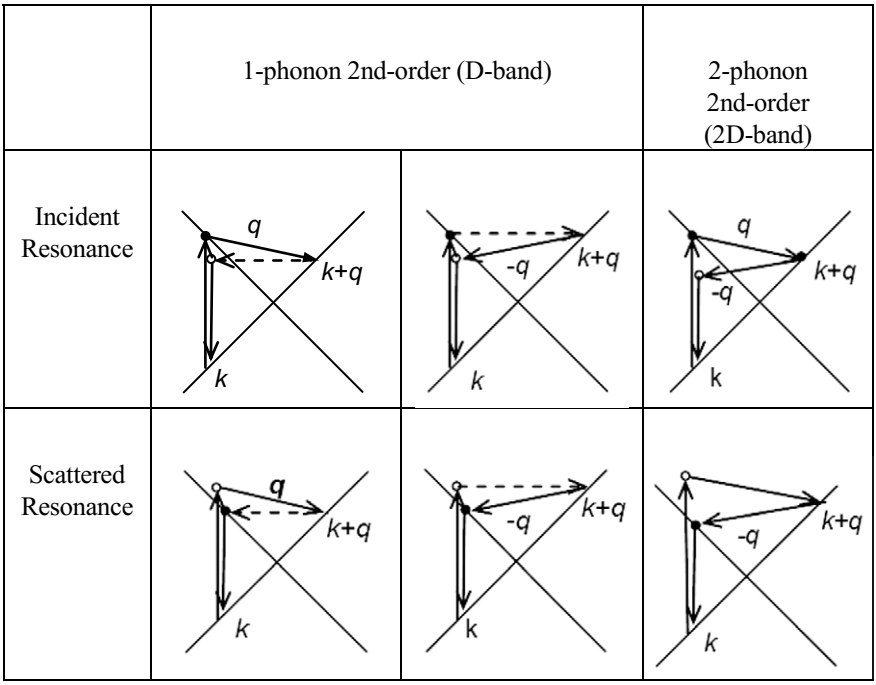

Figure 3.5. Second-order resonance Raman spectral processes for D-band and 2D-band. The dashed lines indicate elastic scattering. Resonance points are shown as solid circles.

In most cases, the 2D-band shows a single Lorentzian peak, but a two-peak 2D-band has also been observed from individual SWNTs. The two-peak structure of 2D-band is observed when two independent double resonance processes are involved. Specifically, for semiconducting SWNTs this occurs when one level of the E_{ii} transition is in resonance with the incident laser while a lower level of interband transition is in resonance with the scattered photon; while for metallic SWNTs, each E_{ii} transition is split into an upper and lower subbands, and both the upper and lower subbands can be involved simultaneously in the two independent resonance processes (Filho et al., 2002a and Filho et al., 2002b). There are 16 (n, m) nanotubes that exhibits a two-peak 2D-band when excited with a 514 nm laser.

For individual SWNTs, the linewidth ranges from 7 to 40 cm^{-1} for the D-band and from 30 to 35 cm^{-1} for the 2D-band. The 2D-band linewidth is a measure of the dispersion state as its value decreases with the decrease of bundle size (Cardenas and Gromov, 2009). The 2D-band position is most sensitive to stress and is usually

employed to follow the deformation of nanotubes. The effect of both the dispersion state and deformation on nanotube Raman bands are important topics in this study and will be discussed next.

3.4. Carbon Nanotube Composites

In view of the impressive mechanical properties of carbon nanotubes, one obvious application of the materials is in the reinforcement of polymer matrices. Examples will now be given of different systems in which SWNTs have been used to produce polymer-based composites (Deng et al., 2011).

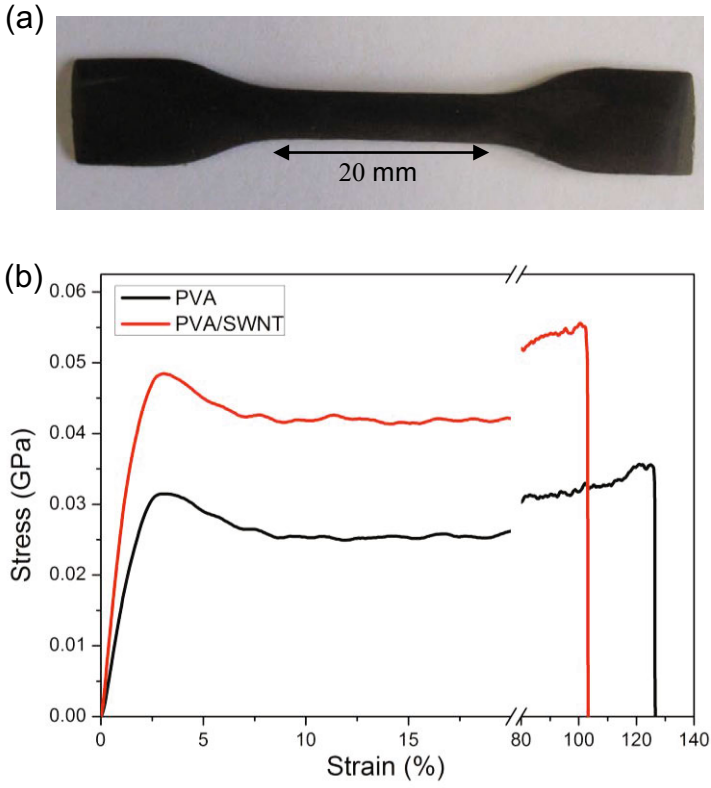

Figure 3.6. Tensile testing of PVT/SWNT nanocomposites. (a) Tensile specimen and (b) stress-strain curves. (Adapted from Deng et al., 2011 with permission from the American Chemical Society).

Table 3.3. Mechanical properties of PVA and PVA/SWNT films (Deng et al., 2011).

Material	Modulus (GPa)	Strength (MPa)	Elongation (%)
PVA	1.9	36	130
PVA/SWNT	2.3	42	110

3.4.1. Bulk SWNT nanocomposites

Bulk composites were prepared consisting of 0.2% by weight of HiPco single-walled carbon nanotubes in a poly(vinyl alcohol) matrix. Tensile specimens were cut out from the as-cast nanocomposite film as shown in Figure 3.6(a). Mechanical testing was carried out with the film samples using an Instron testing machine, and typical stress-strain curves are shown in Figure 3.6(b). For both neat the PVA and PVA/SWNT films, the stress increased linearly with the strain in the low strain range (< 2.5% strain) and the polymers yielded at around 3% strain. The films fractured when the strain exceeds 100%, showing good ductility of the sample. The moduli of the films were calculated in the strain range of 0.5 - 2.5% where good linearity was found. It was found the modulus increase from 1.9 GPa for neat PVA film to 2.3 GPa for PVA/SWNT composite film (see Table 3.3) and the ultimate tensile strength increased from 36 MPa to 42 MPa with just 0.2% of SWNTs in the composite film.

It is also possible to use Raman spectroscopy to follow the deformation of the nanotubes with in the composites. Figure 3.7(a) shows the Raman spectra of the PVA/SWNT composite film and HiPco SWNTs. It can be seen that the spectrum of the nanocomposite is very similar to that to that of the pure nanotubes, even though the nanocomposite only contains 0.2% of SWNTs by weight. This is because the nanotubes undergo very strong resonance Raman scattering (Dresselhaus et al., 2002; Dresselhaus et al., 2005), whereas the PVA matrix only shows weak scattering. It also means that Raman spectroscopy is a very useful technique to analyse many aspects of the structure and properties of nanotube composites.

The PVA/SWNT films were deformed using a four-point bending rig and Figure 3.7(b) shows the 2D-band position as a function of the strain applied to the composites. Good linearity between 2D peak position and strain can be seen over the strain range. The nanotube 2D-band shift per unit strain, observed in the elastic deformation region in PVA/SWNT film, of -23 cm^{-1}/% strain, is the highest found in isotropic polymer/nanotube films. The Raman band shift rate can be converted to the nanotube modulus using a universal calibration of -5 $cm^{-1}\%^{-1}$/GPa. This calibration was established by Cooper et al. (2001) by in-situ Raman spectroscopic study of a number of different carbon fibres. The high band shift rate measured for the PVA/SWNT film implies that the effective Young's modulus of the SWNTs in the nanocomposites is 600 GPa (Deng et al., 2011). It is also similar to the effective modulus of the SWNTs in the film determined from the data in Figure 3.6.

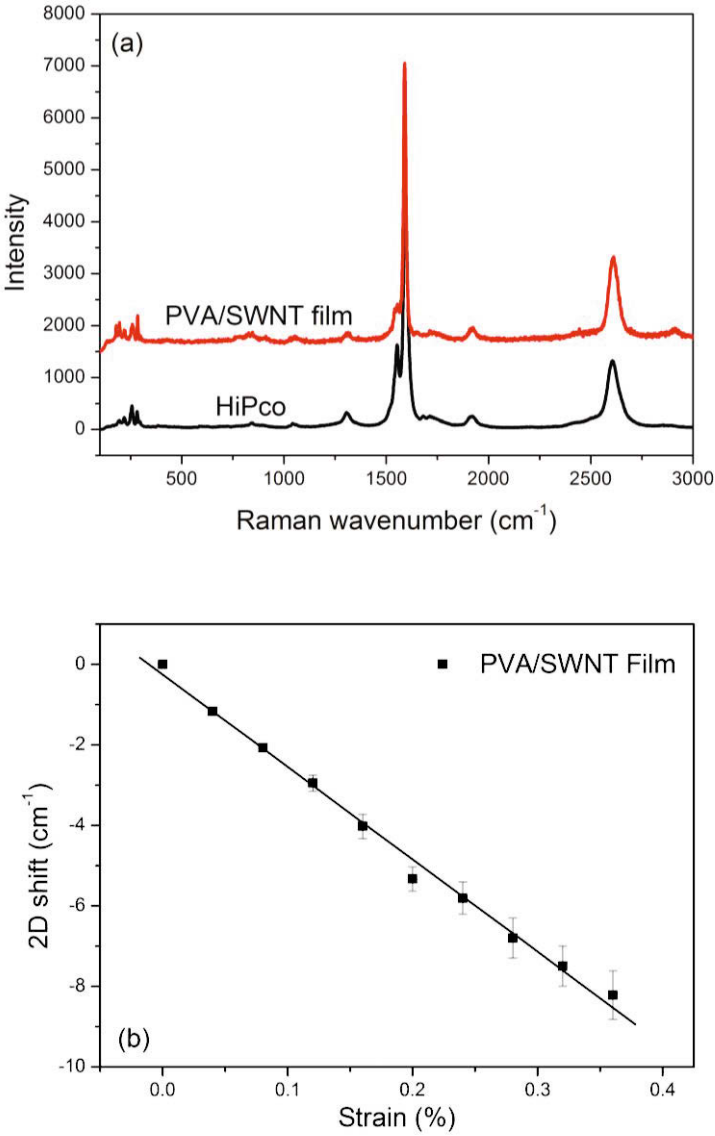

Figure 3.7. (a) Raman spectra of HiPco SWNTs and the PVA/SWNT film. (b) Variation of 2D-band position for nanotube in PVA/SWNT film as a function of strain. (Adapted from Deng et al., 2011 with permission from the American Chemical Society).

3.4.2. SWNT nanocomposites fibres

PVA/SWNT composite fibres containing 0.2% by weight (relative to the polymer) of HiPco SWNTs were prepared by electrospinning (Deng et al., 2011). The spinning conditions were: voltage, 20 kV; flow rate, 0.01 mL/min; and needle tip-to-collector distance, 8 cm. The fibres were collected using either 1) a grounded stationary stage or 2) for deformation studies a rotating disk on which a PMMA beam was attached. The angular velocity of the disk was 1500 rpm.

Narrow-diameter electrospun nanocomposite fibres, an example of which is shown in Figure 3.8, were collected after being aligned macroscopically using the rotating disk. The fibre diameter was controlled by varying the processing conditions such as the concentration of polymer solution, the flow rate and the speed of disk rotation. A range of different fibre diameters were obtained. The average diameter decreased from 700 nm for fibres collected at 0 rpm (a grounded stationary stage) to 590 nm for those collected with a disk rotating at an angular velocity of 1500 rpm. The macroscopic orientation of the fibres collected on the PMMA beam could be controlled by changing the position of the beam on the rotating disk relative to the direction of disc rotation (Deng et al., 2011).

Figure 3.9 shows the Raman spectra of a single PVA/SWNT fibre. Because of the resonantly-enhanced signal from the nanotubes, well-defined Raman bands such as the RBMs, G-band and 2D-band from nanotubes can be seen even at the low loadings of nanotubes employed (0.2%). The strong G band was used to characterize the orientation of the SWNTs in the nanocomposites and the highly stress-sensitive 2D band was employed to follow their deformation.

The 2D-band position in the electrospun fibres collected at 0 rpm was 2 cm^{-1} higher than in the film while the 2D-band position in fibres collected with 1500 rpm was 2 cm^{-1} lower than in the films. This suggests that the electrospinning process alone induces a small residual compression of the nanotubes in the fibres, possibly due to shrinkage as the solvent evaporates. In contrast, in fibres collected with a high-speed rotating disk the nanotubes are pre-stretched and had a slight residual tension that is not relaxed by solvent evaporation. Weak but resolvable Raman bands in the 600-1200 cm^{-1} region corresponding to PVA polymer are shown in the inset. They also enable the orientation of the polymer to be followed through the use of Raman spectroscopy (Deng et al., 2011).

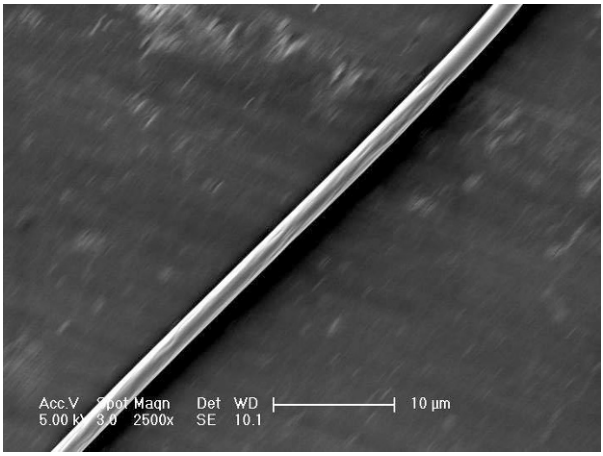

Figure 3.8. SEM micrograph of a single electrospun nancomposite fibre. (Adapted from Deng et al., 2011 with permission from the American Chemical Society).

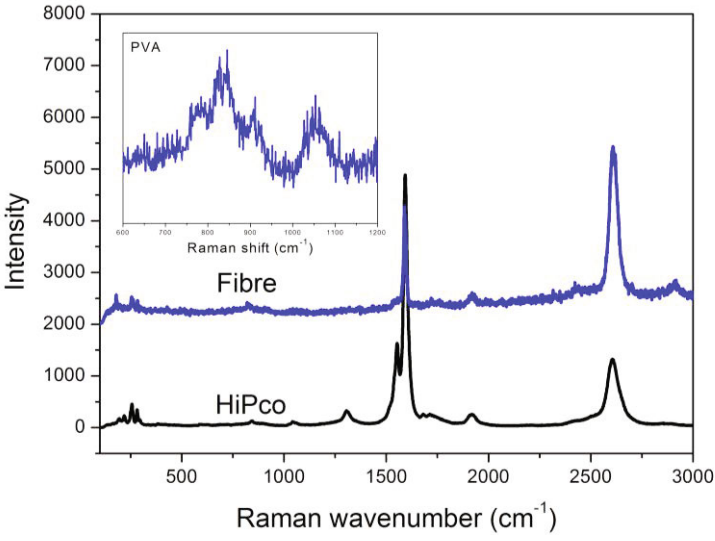

Figure 3.9. Raman spectra obtained from a single electrospun PVA/SWNT fibre and the HiPco nanotubes. The spectra have been offset for clarity and the region of the spectrum showing the PVA bands is inset. (Adapted from Deng et al., 2011 with permission from the American Chemical Society).

The orientation of the nanotubes in the nanofibres was characterized using polarized Raman spectroscopy using VV laser polarization with the incident laser beam and analyser both polarized parallel to the fibre axis (Deng et al., 2011). Figure 3.10 shows the normalized intensity of the nanotube G-band of a single nanocomposite fibre oriented at different angles φ between fibre axis and the laser polarization direction. It can be seen the intensity decreases dramatically as the angle φ increases, indicating a high degree of alignment of the nanotubes in the fibre. The solid line is generated for a relationship of $I \propto \cos^4\varphi$ which is expected to apply for perfect orientation of the nanotubes in the fibre (Liu and Kumar, 2003). The data follow the curve very closely until $\varphi > 60°$ but deviate a little from the theoretical line above this angle, showing some slight misorientation. The strong drawing force exerted by electrical field results in a high draw ratio in electrospinning jets and a high degree of nanotube alignment.

Along with the high degree of orientation of nanotubes achieved in the electrospun fibre, the polymer molecules can also be oriented under the strong electrical forces together with the drawing force exerted by the rotating disk. The ~2 μm diameter laser spot is significantly larger than both the nanotubes and fibre diameter. Hence these measurements determine only the average orientation of the SWNTs – there may be significant local variations of both of these parameters within the nanofibres (Deng et al., 2011).

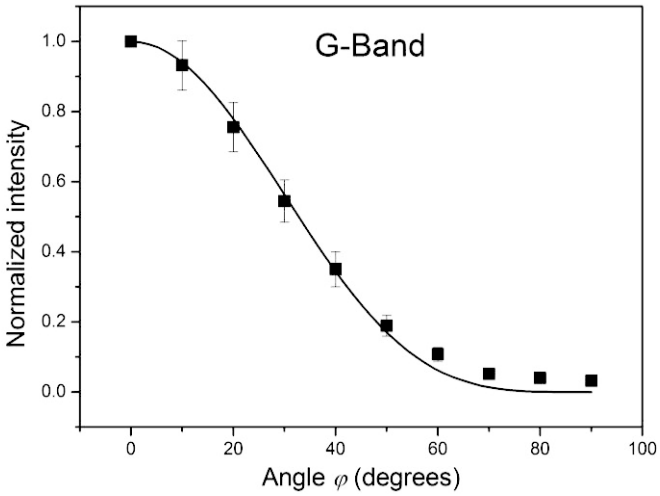

Figure 3.10. Variation of nanotube G-band intensity recorded using the VV configuration, as a function of the angle φ between the fibre axis and the laser polarization direction for an electrospun PVA/SWNT fibre. (Adapted from Deng et al., 2011 with permission from the American Chemical Society).

Figure 3.11 shows the stress induced shift of the G'-band for an electrospun nanofibre. The electrospun fibre exhibited a Raman band shift rate of -35 cm^{-1}/% strain which is higher than that shown for the film in Figure 3.7(b) as a consequence of the better orientation of both the nanotubes and polymer molecules in the nanofibres (Deng et al., 2011). Cooper et al. (2001) measured the Raman band shift rate for the 2D band for a number of different carbon fibres and showed that there was a universal calibration of -5 $cm^{-1}\%^{-1}$/GPa. Assuming that the calibration was also valid for the stress-induced shift of the same 2D band in carbon nanotubes, they used it to determine the effective Young's modulus of both single- and multi-walled carbon nanotubes in epoxy-matrix composites.

The 2D Raman band shift rate can be used to determine the effective modulus of the SWNTs in the electrospun nanofibres and it is again found to be of the order of 600 GPa, i.e. about 60% of the accepted value of around 1000 GPa. The slightly lower value for the nanocomposite films determined from Figure 3.7(b) may be due to all of the nanotubes not lying exactly in the plane of the films. The discrepancy with the accepted value can further be accounted for by factors such as SWNT bundling and finite length effects (Deng et al., 2011).

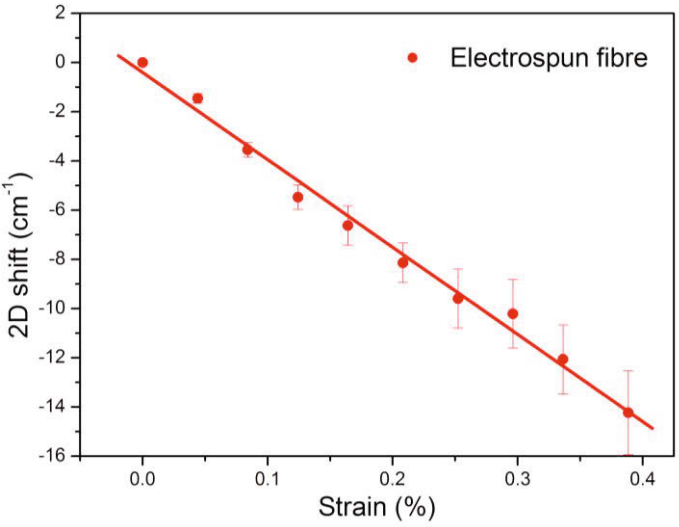

Figure 3.11. Variation of 2D-band position for nanotubes in the PVA/SWNT electrospun fibre as a function of strain. (Adapted from Deng et al., 2011 with permission from the American Chemical Society).

3.4.3. Aramid/nanotube fibres

Poly(p-phenylene terephthalamide)/single-walled carbon (PPTA/SWNT) composite fibres with different draw ratios (DR) were spun using a dry-jet wet spinning process and their structure and deformation behaviour has been analysed using Raman spectroscopy (Deng et al., 2010).

Figure 3.12 shows the Raman spectrum of a neat PPTA fibre, the original carbon nanotubes and a PPTA/SWNT composite fibre. Characteristic bands of both nanotubes and PPTA polymers can be seen from the composite fibres, and this enables the use of Raman spectroscopy for further characterization. Two features have been found by comparing the spectrum of composite and the original SWNTs: 1) The 2D-band from the composite fibre is higher in wavenumber than that from the original SWNTs in air, and fibres with higher DRs show a higher peak position, indicating residual compressive stress in the fibre upon drawing; and 2) The multiple peaks observed in the low-frequency region (radial breathing mode, RBM), together with the peak position and bandwidth of G'-band suggest the nanotubes were still in bundles even the processing condition were optimized to exfoliate nanotubes (Deng et al., 2010).

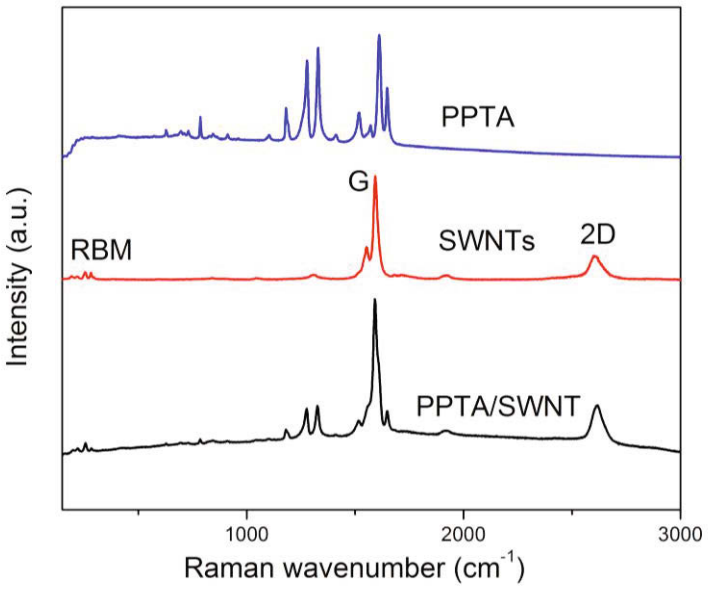

Figure 3.12. Raman spectrum of neat PPTA, SWNTs and PPTA/SWNT composite fibres. (Adapted from Deng et al., 2010 with permission from Elsevier).

The mechanical properties were determined for both the neat PPTA and PPTA/SWNT fibres and typical stress-strain curves are shown in Figure 3.13 for the composite fibres. It can be seen the slope in these curves decreases when the strain exceeds 0.5% and increases after 1%. The variation in modulus is thought to be due to change of the molecular configuration under strain and the variation becomes less pronounced as the DR of fibres increases (Deng et al., 2010).

It was found that the Young's modulus of reinforced fibres was improved by 15% for composite fibres relative to the neat fibres for a DR of 2. For fibres with higher DRs, the mechanical properties were degraded, an effect that has been observed for other high performance polymer/nanotube composites as well. It should be noted that mechanical reinforcement of polymers by nanotubes has been mostly on relatively low modulus polymers such as PVA (Deng et al., 2011). It appears that attempts to reinforce high-performance fibres such as PPTA have been less successful. Mechanical degradation by pristine nanotubes has also been reported where poor dispersion of nanotubes and weak interfacial interactions occur. The use of Raman spectroscopy to follow the mechanisms of stress transfer in the PPTA/SWNT fibres will now be presented.

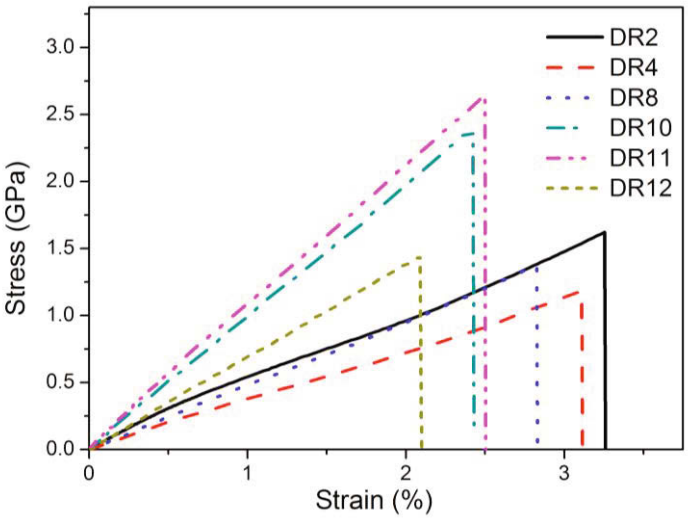

Figure 3.13. Typical stress-strain curves of PPTA/SWNT fibres. (Adapted from Deng et al., 2010 with permission from Elsevier).

In-situ Raman spectroscopy was employed to follow the deformation behaviour of the composite fibres by Deng et al. (2010). Figure 3.14 shows the variation of Raman band positions during tensile deformation. The PPTA 1610 cm^{-1} peak shifted to lower wavenumber linearly with increasing strain up to fibre fracture. On the other hand, the nanotube 2D-band and G-band wavenumbers were found to decrease as the strain increased until it reached 0.35%, and the downshift for both bands ceased when the strain exceeded 0.6%. This indicates breakdown of the interface in the strain range of 0.35-0.6%, which can be a result of interfacial sliding at SWNT-SWNT interface and/or SWNT-polymer interface.

The Raman shift rate increases with the DR of the fibre, and is found to scale with the modulus of the composite fibre. The large band shift rate of nanotube 2D-band within small strain range is clearly an indication of stress transfer from the matrix to the nanotubes. Molecular dynamics simulation carried out by Yang et al. (2005) has demonstrated that strong interfacial adhesion exists between nanotubes and polymers that contain aromatic rings in their backbone, as is the case for PPTA molecules. This strong interfacial interaction should give rise to mechanical reinforcing on PPTA fibres, but is not the case for PPTA/SWNT fibres except for the fibre with a DR of 2. Chang et al. (2006) have also observed the phenomenon that high efficiency of stress transfer results in very limited reinforcement and the reason remained unclear in their work. In the work of Deng et al. (2010), the matrix became degraded compared to the neat PPTA due to the orientation deterioration, which consequently resulted in the negative reinforcing effect in the composite even when good stress transfer was observed.

The overall downshift of nanotube 2D-band in the fibre deformation process reflects the strength of the interface. For fibres with a DR of 11 in which the nanotubes are highly aligned, a maximum down shift of 8 cm^{-1} has been observed. This level of band shift is significantly less than that observed for the PVA/SWNT materials described above. It is difficult to compare the shift rate for different composites system as it depends on the orientation and type (preparation method) of nanotubes, as well as the properties of polymer matrix. Nevertheless, it is clear that the poor level of reinforcement in the case of PPTA/SWNT fibres shows why the material has inferior properties to the PPTA fibres without the nanotubes.

The examples given above show the use of employing stress-induced Raman band shift to characterize stress transfer from polymer matrices to carbon nanotubes in a variety of different composite systems.

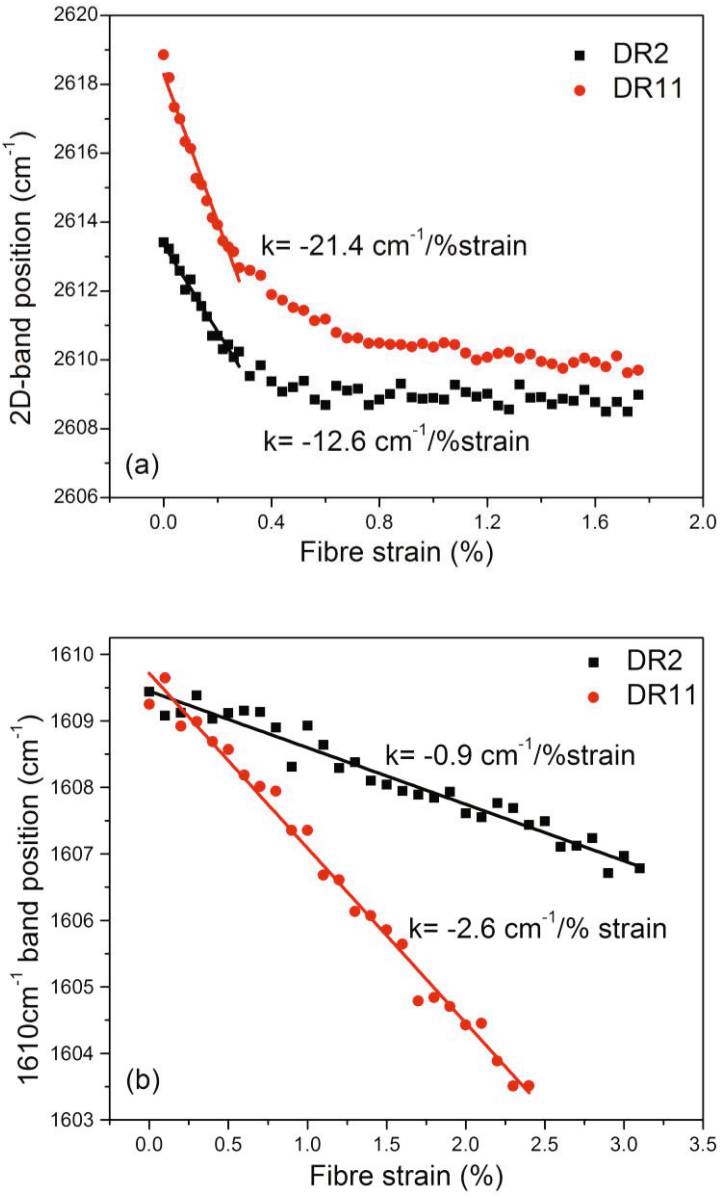

Figure 3.14. Variation of Raman band peak position for composite fibre with different DRs under tensile deformation: a) nanotube 2D-band and b) PPTA 1610 cm^{-1} peak. (Adapted from Deng et al., 2010 with permission from Elsevier).

3.5. Conclusions

It has been shown that carbon nanotubes have a range of different well-defined nanostructures that control their electronic and mechanical properties. Moreover, it has been demonstrated that Raman spectroscopy is a powerful technique to characterize the nanotubes and the origin of the different Raman bands found in nanotubes has been discussed in detail.

The deformation behaviour of the nanotubes in both PVA/SWNT composite films produced by solution casting and composite fibres fabricated by electrospinning and coagulation spinning has been discussed. Significant levels of reinforcement were shown to be found upon the addition of carbon nanotubes, even at loading levels as low as 0.2% by weight.

Raman spectroscopy has again been demonstrated to be extremely powerful in characterizing the deformation of these PVA/SWNT composite materials. Large Raman band shift rates were observed in the composite film and electrospun fibres corresponding to high levels of stress transfer between the polymer matrix and the nanotubes. This good stress transfer was shown to the consistent with the bulk mechanical properties of the PVA/SWNT composite materials.

The modification of aramid fibres with the addition of carbon nanotubes has also been described. Although it is demonstrated that through the use of Raman spectroscopy, reasonable levels of stress transfer are found between the aramid matrix and the nanotubes, it is found that there is generally poor reinforcement in this system due to slippage of the nanotubes at high strain levels.

Overall it has been shown that Raman spectroscopy is a powerful technique to characterize a range of important aspects of the structure and properties of carbon nanotubes.

References

Araujo P. T., Doorn S. K., Kilina S., Tretiak S., Einarsson E., Maruyama S., Chacham H., Pimenta M. A., and Jorio A. (2007) Third and fourth optical transitions in semiconducting carbon nanotubes. *Physical Review Letters*, 98:067401 1-4.

Bachilo S., Strano M., Kittrell C., Hauge R., Smalley R., and Weisman R. (2002). Structure-Assigned Optical Spectra of Single-Walled Carbon Nanotubes. *Science*, 298:2361-2366.

Bose S. M., Gayen S., and Behera S. N. (2005). Theory of the tangential G-band feature in the Raman spectra of metallic carbon nanotubes. *Physical Review B*, 72:153402 1-4.

Cardenas J., and Gromov A. (2009). The effect of bundling on the G' Raman band of single-walled carbon nanotubes. *Nanotechnology*, 20:465703 1-8.

Chang T. E., Kisliuk A., Rhodes S. M., Brittain W. J. and Sokolov A. P. (2006). Conductivity and mechanical properties of well-dispersed single-wall carbon nanotube/polystyrene composite. *Polymer*, 47:7740-7746.

Coleman J., Khan U., Blau W., and Gun'Ko Y. (2006a). Small but strong: A review of the mechanical properties of carbon nanotube–polymer composites. *Carbon*, 44:1624-1652.

Coleman J., Khan U., Blau W., and Gun'Ko Y. (2006b). Mechanical reinforcement of polymers using carbon nanotubes, *Advanced Materials*, 18:689-706.

Cooper C. A., Young R. J., and Halsall M. (2001). Investigation into the deformation of carbon nanotubes and their composites through the use of Raman spectroscopy. *Composites A: Applied Science and Manufacturing*, 32:401-411.

Deng L. B., Young R. J., van der Zwaag S., and Picken S. (2010). Characterization of the adhesion of single-walled carbon nanotubes in poly (*p*-phenylene terephthalamide) composite fibres, *Polymer*, 51:2033-2039.

Deng L. B., Eichhorn S. J., Kao C. C., and Young R. J. (2011). The effective Young's modulus of carbon nanotubes in composites, *ACS Applied Materials & Interfaces*, 3:433-440.

Doorn S. K., Strano M. S., Haroz E. H., Rialon K. L., Hauge R. H., and Smalley R. E. (2003). Capillary electrophoresis separations of bundled and individual carbon nanotubes. *Journal of Physical Chemistry B*, 107:6063-6069.

Dresselhaus M, Dresselhaus G, Jorio A, Souza A and Saito R (2002), Raman spectroscopy on isolated single wall carbon nanotubes, *Carbon*, 40, 2043-2061.

Dresselhaus M., Dresselhaus G., Saito R., and Jorio A. (2005). Raman spectroscopy of carbon nanotubes, *Physics Reports*, 409:47-99.

Fantini C., Jorio A., Souza M., Strano M. S., Dresselhaus M. S., and Pimenta M. A. (2004). Optical transition energies for carbon nanotubes from resonant Raman spectroscopy: Environment and temperature effects. *Physical Review Letters*, 93:147406 1-4.

Filho A. G. S., Jorio A., Dresselhaus M. S., Hafner J. H., Lieber C. M., and Pimenta M. A. (2002a). Probing the electronic trigonal warping effect in individual single-wall carbon nanotubes using phonon spectra. *Chemical Physics Letters*, 354:62-68.

Filho A. G. S., Jorio A., Swan A. K., Ünlü M. S., Goldberg B. B., Saito R., Hafner J. H., Lieber C. M., Pimenta M. A., Dresselhaus G., and Dresselhaus M. S. (2002b), Anomalous two-peak G-band Raman effect in one isolated single-wall carbon nanotube. *Physical Review B*, 65:085417 1-6.

Filho A. G. S., Jorio A., Samsonidze G., Dresselhaus G., Pimenta M. A., Dresselhaus M. S., Swan A. K., Ünlü M., Goldberg B. B., and Saito R. (2003). Competing spring constant versus double resonance effects on the properties of dispersive modes in isolated single-wall carbon nanotubes. *Physical Review B*, 67:035427 1-7.

Heller D. A., Barone P. W., Swanson J. P., Mayrhofer R. M., and Strano M. S. (2005). Using Raman spectroscopy to elucidate the aggregation state of single-walled carbon nanotubes. *Journal of Physical Chemistry B*, 108:6905-6909.

Jorio A., Saito R., Hafner J. H., Lieber C. M., Hunter M., McClure T., Dresselhaus G., and Dresselhaus M. S. (2001). Structural (*n, m*) determination of isolated single-wall carbon nanotubes by resonant Raman scattering. *Physical Review Letters*, 86:1118-1121.

Kataura H., Kumazawa Y., Maniwa Y., Umezu I., Suzuki S., Ohtsuka Y., and Achiba Y. (1999). Optical properties of single-wall carbon nanotubes. *Synthetic Metals*, 103:2555-2558.

Kawamoto H., Uchida H., Kojima T., and Tachibana M. (2006). G band Raman features of DNA-wrapped single-wall carbon nanotubes in aqueous solution and air. *Chemical Physics Letters*, 432:172-176.

Liu T. and Kumar S. (2003). Quantitative characterization of SWNT orientation by polarized Raman spectroscopy. *Chemical Physics Letters*, *378*:257-262

Lu J. P. (1997). Elastic properties of single and multilayered nanotubes. *Journal of the Physical Chemistry of Solids*, 58:1649-1652.

Lucas M., and Young R. J. (2007). Unique identification of single-walled carbon nanotubes in composites. *Composites Science and Technology*, 67:2135–2149.

Milnera M., Kurti J., Hulman M., and Kuzmany H. (2000). Periodic resonance excitation and intertube interaction from quasicontinuous distributed helicities in single-wall carbon nanotubes. *Physical Review Letters*, 84:1324-1327.

Moniruzzaman M., and Winey K. (2006). Polymer nanocomposites containing carbon nanotubes. *Macromolecules*, 39:5194-5205.

O'Connell M. J., Sivaram S., and Doorn S. K. (2004). Near-infrared resonance Raman excitation profile studies of single-walled carbon nanotube intertube interactions: A direct comparison of bundled and individually dispersed HiPco nanotubes, *Physical Review B*, 69:235415 1-15.

Paillet M., Poncharal P., Zahab A., and Sauvajol J. L. (2005). Vanishing of the Breit-Wigner-Fano component in individual single-wall carbon nanotubes. *Physical Review Letters*, 94:237401 1-4.

Saito R., Dresslhaus G., and Dressihaus M. (1998). *Physical properties of carbon nanotubes*, London: Imperial College Press.

Treacy M. M., Ebbesen T. W., and Gibson T. M. (1996). Exceptionally high Young's modulus observed for individual carbon nanotubes. *Nature*, 381:680-687.

Wise K. E., Park C., Siochi E. J., and Harrison J. S. (2004). Stable dispersion of single wall carbon nanotubes in polyimide: the role of noncovalent interactions. *Chemical Physics Letters*, 391:207-211.

Wong E. W., Sheehan P. E., and Lieber C. M. (1997). Nanobeam mechanics: Elasticity, strength, and toughness of nanorods and nanotubes. *Science*, 277:1971-1975.

Yang M. J., Koutsos V., and Zaiser M. (2005). Interactions between polymers and carbon nanotubes: A molecular dynamics study. *Journal of Physical Chemistry B*, 109:10009 – 10014.